

Ultra-sensitive Parity-Time Symmetry based Graphene FET (PTS-GFET) Sensors

Lu Ou

College of Computer Science and Electronic Engineering
Hunan University
Changsha, Hunan, China
oulu9676@gmail.com

Shaolin Liao*

Department of Electrical and Computer Engineering
Illinois Institute of Technology
Chicago, IL, USA
sliao5@iit.edu; ORCID: 0000-0002-4432-3448

Abstract—A novel ultra-sensitive Parity-Time symmetry based Graphene FET (PTS-GFET) sensor is studied for gas concentration detection. The PTS-GFET sensor effectively integrates the sensitivity of the PT symmetry around its Exceptional Point (EP) and the tunability of the GFET conductance. The change of GFET conductance with the gas concentration can be brought back to the EP of the PTS-GFET by tuning the gate voltage on the GFET. Thus, the applied gate voltage indicates the gas concentration. The minimum detectable gas concentration has been derived and estimated based on the experimental data, which shows that PTS-GFET can detect gas concentration below 50 ppb.

Index Terms—Parity-Time (PT) symmetry, graphene Field Effect Transistor (GFET), tunable gas sensors.

I. INTRODUCTION

Tunable Graphene Field Effect Transistor (GFET) can be used as resistance based sensitive sensors to measure ppb-level concentrations of gases such as NO₂ and NH₃ [1]. However, working at low-frequency is prone to the 1/*f* noise, which reduces the sensitivity of the GFET sensors.

Sensors working at the electromagnetic frequency [2]–[30] can eliminate the 1/*f* noise to improve the sensors' performance. In addition, bandpass filters of high quality factor *Q* can be used to further reduce the out-of-band noise.

What's more, the emerging Parity-Time (PT) symmetry phenomenon at the electromagnetic frequency [31] can be explored to build very sensitive sensors around its Exceptional Point (EP), where the gain and loss balance each other and the ideal frequency splitting becomes zero.

In this paper, we study an ultra-sensitive PT symmetry based GFET (PTS-GFET) gas sensor by integrating the sensitivity of the PT symmetry around its EP and the tunability of the GFET.

II. THE PTS-GFET GAS SENSOR

Fig. 1 shows the concept of the PTS-GFET: it consists of a coupled RLC resonator pair, *i.e.*, the ($-G_1, L_1, C_1$) resonator on the reading side and the (G_2, L_2, C_2) on the

GFET sensing side. Ideally, the individual resonant frequencies of ($-G_1, L_1, C_1$) and (G_2, L_2, C_2) are identical, *i.e.*, $\omega_1 = \omega_2 = 1/\sqrt{L_1 C_1}$. The negative conductance $-G_1$ is realized through a feedback amplifier [32]. The conductance of the GFET G_2 changes with the gas concentration c_{gas} , as shown by the O-A path on the left plot of Fig. 2. To bring the PTS-GFET back to the EP, a gate voltage V_G is applied to the GFET so that the changed GFET conductance G_2 is brought back to its origin, as shown by the A-B path on the left plot of Fig. 2. A Vector Network Analyzer (VNA) is used to scan the reflection spectrum to monitor that the PTS-GFET is actually brought back to the EP condition, *i.e.*, $G_1 = -G_2$. Finally, the gate voltage V_G will indicate the gas concentration c_{gas} .

III. THE COUPLED RLC COIL RESONATORS

The PTS-GFET can be modeled as a coupled resonator pair. Each resonator can be modeled as a RLC resonant tank that consists of 3 components in parallel: an inductor with inductance *L*, a capacitor with capacitance *C* and a resistor *R*.

A. The Governing Equations System

When a pair of RLC resonant tanks are brought close to each other, they are coupled together through magnetic flux of the two inductive coils, which can be characterized by the mutual inductance *M*. The coupled resonant coils can be analyzed by the physical quantities of currents i_1/i_2 and voltages v_1/v_2 through the indicators of the two coupled coil resonators,

$$v_1 = L_1 \frac{di_1}{dt} + M \frac{di_2}{dt}, v_2 = L_2 \frac{di_2}{dt} + M \frac{di_1}{dt}. \quad (1)$$

The Kirchhoff Current Law (KCL) connects the currents through the inductor with inductance *L*, the capacitor with capacitance *C* and the resistor with conductance *G* as follows,

$$i_1 + C_1 \frac{dv_1}{dt} + G_1 v_1 = 0, i_2 + C_2 \frac{dv_2}{dt} + G_2 v_2 = 0. \quad (2)$$

*Shaolin Liao is the corresponding author.

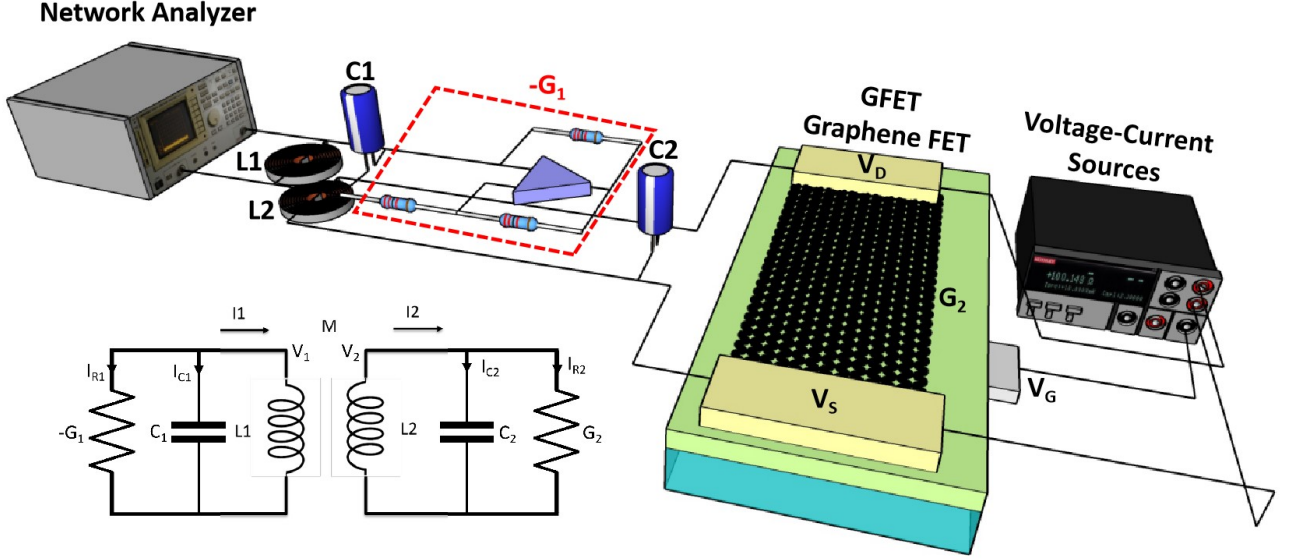


Fig. 1. The PTS-GFET sensor concept and working principle: it consists of two RLC resonators, denoted by $(-G_1, L_1, C_1)$ and (G_2, L_2, C_2) . A VNA is used to obtain the reflection spectrum to find the EP of the PTS-GFET when the conductance of the GFET is tuned by the gate voltage through a voltage-current source, in an effort to cancel the effect of the gas concentration. Also, the bottom diagram shows the working principle of the PTS-GFET modeled as the coupled RLC resonators.

B. The Quantum Hamiltonian

In our recent paper [33], rigorous quantum Hamiltonian for the coupled RLC coil resonators system has been derived through twice basis transforms of the original basis. The first basis transform rotates the original basis such that off-diagonal terms of the governing matrix of the equation system of the coupled coil resonators reduces to constants. Then a second basis transform obtains the quantum Hamiltonian, including the diagonal effective complex frequencies and the off-diagonal coupling terms, together with the transformed basis. In particular, for identical and lossless coupled RLC resonators, *i.e.*, $\omega_1 = \omega_2 = 1/\sqrt{L_1 C_1}$ and $G_1 = G_2 = 0$, the quantum Hamiltonian reads,

$$\mathcal{H}_0 = \begin{bmatrix} \Omega & 1 \\ 1 & \Omega \end{bmatrix}, \quad (3)$$

where $\Omega = \omega/\kappa$ is the normalized complex frequency and κ is the effective coupling strength.

For identical PT-symmetric coupled RLC resonators, *i.e.*, $\omega_1 = \omega_2 = 1/\sqrt{L_1 C_1}$ and $G_2 = -G_1 = G$, the effective quantum Hamiltonian can be expressed as

$$\mathcal{H}_{PT} = \begin{bmatrix} \Omega + jg & 1 \\ 1 & \Omega - jg \end{bmatrix}, \quad (4)$$

where $g = G/(2\kappa)$ is the normalized conductance.

If the coupled RLC resonators deviates in their own resonant frequencies and the gain doesn't balance the loss,

i.e., $\omega_1 \neq \omega_2$ and $G_1 \neq -G_2$, the quantum Hamiltonian of Eq. (4) can be expressed as follows [34],

$$\mathcal{H}'_{PT} = \begin{bmatrix} \Omega + \Delta - jg' & 1 \\ 1 & \Omega - \Delta + jg \end{bmatrix}, \quad (5)$$

where $\Delta = (\omega_1 - \omega_2)/(2\kappa)$ is the normalized frequency deviation of the two RLC resonators.

C. The Eigenfrequencies

The eigenfrequencies of the quantum Hamiltonian of Eq. (5) are given by,

$$\Omega_{\pm} = \Omega + j\frac{g-g'}{2} \pm \sqrt{1 - \left(\frac{g+g'}{2} + j\Delta\right)^2}. \quad (6)$$

We are interested in the EP regime where $g' = 1$; $g \sim 1$, which is realized through tuning the gate voltage V_G of the GFET. For the normalized frequency deviation $\Delta \sim 0$, the eigenfrequencies of Eq. (6) can be approximated as follows,

$$\begin{aligned} \Omega_{\pm} &= \left(\Omega \pm \sqrt{1 - (1 - \Delta g/2)^2} \right) - j\Delta g/2, \\ &\sim \left(\Omega \pm \sqrt{\Delta g} \right) - j\Delta g/2, \end{aligned} \quad (7)$$

where $\Delta g = 1 - g$.

Assuming that the GFET conductance change δg is much smaller than its Gaussian noise fluctuation standard deviation σ , *i.e.*, $\delta g \ll \sigma$, it can be shown [34] that the normalized PT frequency splitting sensitivity is given by,

$$s_{\Omega} \equiv \sqrt{\frac{\pi\sigma}{2}} = \sqrt{\frac{\pi\sigma}{2} \frac{\partial \langle \Omega_+ - \Omega_- \rangle}{\partial \Delta g}} \sim \frac{\Delta g}{\sigma}. \quad (8)$$

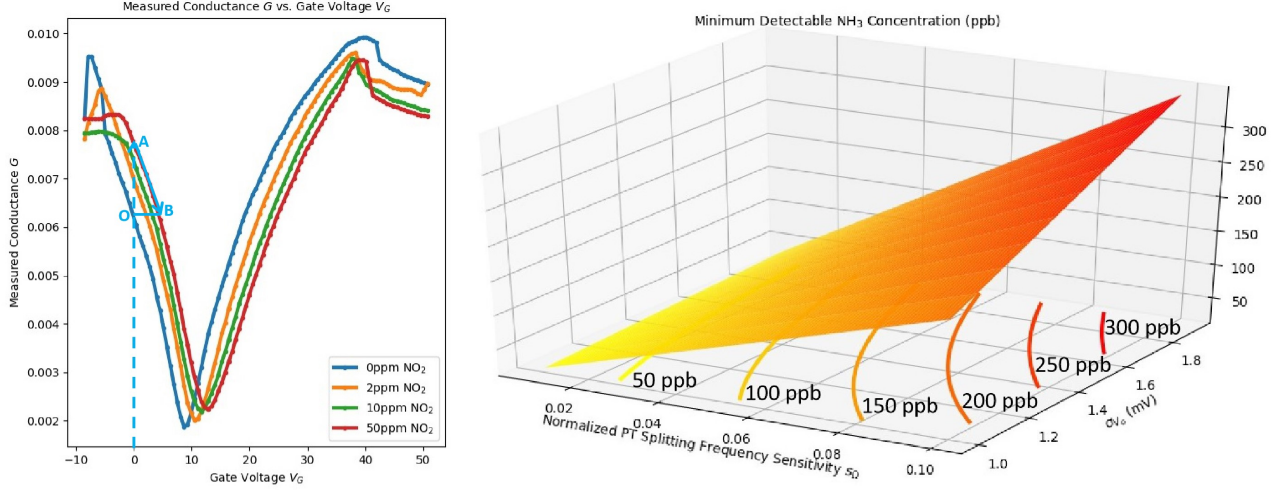


Fig. 2. Conductance/resistance of GFET exposed to the NH_3 gas of different concentrations: left) Drain-source current I vs. gate voltage V_G ; and 2) the estimated minimum detectable gas concentration c_{gas} calculated from the experimental data.

IV. THE TUNABLE GFET

It is well-known that the conductance of the GFET G can be tuned by applying the gate voltage V_G . In practical experimental environment, due to fluctuation of the gate voltage δV_G , the GFET's normalized noisy conductance $\delta g = \delta G / (2\kappa)$ given by,

$$\delta g = \frac{\delta G}{2\kappa} = \frac{\partial g}{\partial V_G} \delta V_G, \quad (9)$$

from which the standard deviation of the normalized noisy conductance δg , denoted as σ , is obtained as follows,

$$\sigma = \frac{\partial g}{\partial V_G} \sigma_{V_G}, \quad (10)$$

where σ_{V_G} is the standard deviation of the gate voltage V_G .

V. THE MINIMUM DETECTABLE GAS CONCENTRATION

The change of the graphene conductance Δg due to the change of the gas concentration Δc is given by,

$$\Delta g = \frac{\partial g}{\partial c_{gas}} \Delta c_{gas}. \quad (11)$$

Substituting Eq. (10) and Eq. (11) into Eq. (8), the normalized PT frequency splitting sensitivity due to the gate voltage fluctuation δV_G is obtained,

$$s_\Omega \sim \frac{\frac{\partial g}{\partial c_{gas}}}{\frac{\partial g}{\partial V_G} \sigma_{V_G}} \Delta c_{gas}, \quad (12)$$

from which the minimum detectable gas concentration is given by,

$$\Delta c_{gas} \sim \frac{\frac{\partial g}{\partial V_G} \sigma_{V_G}}{\frac{\partial g}{\partial c_{gas}}} s_\Omega. \quad (13)$$

We have estimated the minimum detectable gas concentration c_{gas} based on the experimental data: 1) the change of GFET conductance with respect to the gate voltage $\partial g / \partial V_G$ is obtained from the measured GFET conductance vs. the gate voltage V_G , as shown on the left plot of Fig. 2; and 2) the change of the GFET conductance vs. the gas concentration c_{gas} of NO_2 is obtained from the literature [1]. Finally, the estimated minimum detectable gas concentration c_{gas} for different gate voltage noise standard deviation σ_{V_G} and normalized PT splitting frequency deviation s_Ω is shown on the right plot of Fig. 2. It can be seen that the minimum detectable gas concentration $c_{gas} < 50$ ppb when the gate voltage noisy deviation $\sigma_{V_G} = 1\text{mV}$ and the normalized PT splitting frequency sensitivity $s_\Omega < 0.02$.

VI. CONCLUSION

In this paper, an ultra-sensitive PTS-GFET sensor has been studied for gas concentration detection. The PTS-GFET effectively integrates the sensitivity of the PT symmetry phenomenon and the tunability of the GFET to form an ultra-sensitive sensor. Minimum detectable gas concentration has been analyzed. A minimum detectable gas concentration of < 50 ppb has been estimated from the experimental data, showing that the PTS-GFET sensor is very promising in detecting tiny change of GFET conductance induced by physical parameters such as gas concentration, solute concentration in liquid and ultraviolet photons.

REFERENCES

- [1] F. Yavari, E. Castillo, H. Gullapalli, P. M. Ajayan, and N. Koratkar, "High sensitivity detection of NO_2 and NH_3 in air using chemical vapor deposition grown graphene," Appl. Phys. Lett., vol. 100, no. 20, p. 203120, May 2012.

- [2] Shaolin Liao and R. J. Vernon. On the Image Approximation for Electromagnetic Wave Propagation and PEC Scattering in Cylindrical Harmonics. Progress In Electromagnetics Research, 66:65-88, 2006. Publisher: EMW Publishing.
- [3] Shaolin Liao and Ronald J. Vernon. The Near-Field and Far-Field Properties of the Cylindrical Modal Expansions with Application in the Image Theorem. In 2006 Joint 31st International Conference on Infrared Millimeter Waves and 14th International Conference on Terahertz Electronics, pages 260-260, September 2006. ISSN: 2162-2035.
- [4] Shaolin Liao and R.J. Vernon. A new fast algorithm for calculating near-field propagation between arbitrary smooth surfaces. In 2005 Joint 30th International Conference on Infrared and Millimeter Waves and 13th International Conference on Terahertz Electronics, volume 2, pages 606-607 vol. 2, September 2005. ISSN: 2162-2035.
- [5] Shaolin Liao, Henry Soekmadji, and Ronald J. Vernon. On Fast Computation of Electromagnetic Wave Propagation through FFT. In 2006 7th International Symposium on Antennas, Propagation EM Theory, pages 1-4, October 2006.
- [6] Shaolin Liao and Ronald J. Vernon. The Cylindrical Taylor-Interpolation FFT Algorithm. In 2006 Joint 31st International Conference on Infrared Millimeter Waves and 14th International Conference on Terahertz Electronics, pages 259-259, September 2006. ISSN: 2162-2035.
- [7] Shaolin Liao. Beam-shaping PEC Mirror Phase Corrector Design. PIERS Online, 3(4):392-396, 2007.
- [8] Shaolin Liao. Fast Computation of Electromagnetic Wave Propagation and Scattering for Quasi-cylindrical Geometry. PIERS Online, 3(1):96-100, 2007.
- [9] Shaolin Liao. On the Validity of Physical Optics for Narrow-band Beam Scattering and Diffraction from the Open Cylindrical Surface. PIERS Online, 3(2):158-162, 2007.
- [10] Shaolin Liao, Ronald J. Vernon, and Jeffrey Neilson. A high-efficiency four-frequency mode converter design with small output angle variation for a step-tunable gyrotron. In 2008 33rd International Conference on Infrared, Millimeter and Terahertz Waves, pages 1-2, September 2008. ISSN: 2162-2035.
- [11] S. Liao, R. J. Vernon, and J. Neilson. A four-frequency mode converter with small output angle variation for a step-tunable gyrotron. In Electron Cyclotron Emission and Electron Cyclotron Resonance Heating (EC-15), pages 477-482. WORLD SCIENTIFIC, April 2009.
- [12] Ronald J. Vernon. High-Power Microwave Transmission and Mode Conversion Program. Technical Report DOEUW52122, Univ. of Wisconsin, Madison, WI (United States), August 2015.
- [13] Shaolin Liao. Multi-frequency beam-shaping mirror system design for high-power gyrotrons: theory, algorithms and methods. Ph.D. Thesis, University of Wisconsin at Madison, USA, 2008. AAI3314260 ISBN-13: 9780549633167.
- [14] Shaolin Liao and Ronald J. Vernon. A Fast Algorithm for Wave Propagation from a Plane or a Cylindrical Surface. International Journal of Infrared and Millimeter Waves, 28(6):479-490, June 2007.
- [15] S.-L. Liao and R. J. Vernon. Sub-THz Beam-Shaping Mirror System Designs for Quasi-optical Mode Converters in High-power Gyrotrons. Journal of Electromagnetic Waves and Applications, 21(4):425-439, January 2007. Publisher: Taylor & Francis.
- [16] Shaolin Liao. Miter Bend Mirror Design for Corrugated Waveguides. Progress In Electromagnetics Research, 10:157-162, 2009. Publisher: EMW Publishing.
- [17] Shaolin Liao and Ronald J. Vernon. A Fast Algorithm for Computation of Electromagnetic Wave Propagation in Half-Space. IEEE Transactions on Antennas and Propagation, 57(7):2068-2075, July 2009. Conference Name: IEEE Transactions on Antennas and Propagation.
- [18] Shaolin Liao, N. Gopalsami, A. Venugopal, A. Heifetz, and A. C. Raptis. An efficient iterative algorithm for computation of scattering from dielectric objects. Optics Express, 19(4):3304-3315, February 2011. Publisher: Optical Society of America.
- [19] Shaolin Liao. Spectral-domain MOM for Planar Meta-materials of Arbitrary Aperture Wave-guide Array. In 2019 IEEE MTT-S International Conference on Numerical Electromagnetic and Multiphysics Modeling and Optimization (NEMO), pages 1-4, May 2019.
- [20] Liao, S., Vernon, R. J. and Neilson, J. A high-efficiency four-frequency mode converter design with small output angle variation for a step-tunable gyrotron. In Proc. 33rd International Conference on Infrared, Millimeter & Terahertz Waves 1-2 (2008).
- [21] Chan, W. L., et al. A single-pixel terahertz imaging system based on compressed sensing. Appl. Phys. Lett. **93**, 121105 (2008).
- [22] Liao, S., and Vernon, R. J. Sub-THz beam-shaping mirror system designs for quasi-optical mode converters in high-power gyrotrons. J. Electromagn. Waves Appl. **21**, 425-439 (2007).
- [23] Bakhtiari, S. et al. A real-time heart rate analysis for a remote millimeter wave I-Q sensor. IEEE Trans. Biomed. Eng. **58**, 1839-1845 (2011).
- [24] Liao, S. et al. A novel interferometric millimeter wave Doppler radar architecture. In Proc. 2013 IEEE International Instrumentation and Measurement Technology Conference (I2MTC) 387-391 (IEEE, 2013).
- [25] Liao, S. et al. A novel interferometric Sub-THz Doppler radar With a continuously oscillating reference arm. IEEE Trans. Terahertz Sci. Technol. **4**, 307-313 (2014).
- [26] Liao, S. et al. four-frequency mode converter with small output angle variation for a step-tunable gyrotron. In Proc. Electron Cyclotron Emission and Electron Cyclotron Resonance Heating (EC-15) 477-482 (WORLD SCIENTIFIC, 2009).
- [27] Gopalsami, N. et al. Passive millimeter-wave imaging with compressed sensing. Opt. Eng. **51**, 091614 (2012).
- [28] Babacan, S. D. et al. Compressive passive millimeter-wave imaging. In Proc. 18th IEEE International Conference on Image Processing 2705-2708 (IEEE, 2011).
- [29] Gopalsami, N. et al. Compressive sampling in active and passive millimeter-wave imaging. In Proc. 2011 International Conference on Infrared, Millimeter & Terahertz Waves 1-2 (2011).
- [30] Gopalsami, N. et al. Compressive sampling in passive millimeter-wave imaging. Proceedings of SPIE-The International Society for Optical Engineering **8022**, (18), 1684-1687 (2011).
- [31] M. Hajizadegan, M. Sakhdari, S. Liao, and P.-Y. Chen, High-Sensitivity Wireless Displacement Sensing Enabled by PT-Symmetric Telemetry, IEEE Transactions on Antennas and Propagation, vol. 67, no. 5, pp. 34453449, May 2019.
- [32] Y. J. Zhang et al., Noninvasive Glucose Sensor Based on Parity-Time Symmetry, Phys. Rev. Applied, vol. 11, no. 4, p. 044049, Apr. 2019.
- [33] Shaolin Liao and Lu Ou, "Rigorous Quantum Formulation of Parity-Time Symmetric Coupled Resonators," arXiv:2007.01462: <https://arxiv.org/abs/2007.01462>
- [34] N. A. Mortensen, P. a. D. Gonalves, M. Khajavikhan, D. N. Christodoulides, C. Tserkezis, and C. Wolff, Fluctuations and noise-limited sensing near the exceptional point of parity-time-symmetric resonator systems, Optica, OPTICA, vol. 5, no. 10, pp. 13421346, Oct. 2018.